GRATING LOBE ELIMINATION IN STEERABLE PARAMETRIC LOUDSPEAKER

Chuang Shi and Woon-Seng Gan, *Senior Member, IEEE*

School of Electrical and Electronic Engineering, Nanyang Technological University, Singapore

(e-mail: shic0002@e.ntu.edu.sg; ewsgan@ntu.edu.sg)

ABSTRACT

In the past two decades, majority of researches on the parametric loudspeaker concentrate on the nonlinear modeling of acoustic propagation and pre-processing techniques to reduce nonlinear distortion in sound reproduction. There are however very few studies on directivity control of the parametric loudspeaker. In this paper, we propose an equivalent circular Gaussian source array that approximates the directivity characteristics of the linear ultrasonic transducer array. By using this approximation, the directivity of the sound beam from the parametric loudspeaker can be predicted by the product directivity principle. New theoretical results, which are verified through measurements, are presented to show the effectiveness of the delay-and-sum beamsteering structure for the parametric loudspeaker. Unlike the conventional loudspeaker array, where the spacing between array elements must be less than half the wavelength to avoid spatial aliasing, the parametric loudspeaker can take advantage of grating lobe elimination to extend the spacing of ultrasonic transducer array to more than one and a half wavelength in a typical application.

Key Words: *Beamsteering, spatial aliasing, ultrasonic transducer array, parametric loudspeaker, nonlinear acoustics.*

I. INTRODUCTION

Due to the high directivity of sound beams created by the parametric loudspeaker, it can be deployed in many sound confinement applications, such as providing personal listening zones in public area and creating immersive sound effects in virtual reality [1]. The principle of the parametric loudspeaker, commonly known as parametric array, was first theoretically explained by Westervelt [2] in 1963. Since then many studies were investigated in underwater. It is not until 1975 when Bennett and Blackstock [3] proved that parametric array is also able to operate in air. Yoneyama and Fujimoto [4] later demonstrated that the parametric loudspeaker can be used to create a directional audio beam by amplitude modulating a high intensity ultrasonic carrier signal with audio signal. However, severe distortion was observed, and subsequently, different types of preprocessing methods and modulation techniques [5]-[8] have been studied to reduce the distortion to an acceptable speech quality level.

Several theoretical models are currently used in describing the nonlinear acoustics properties of parametric array [9]-[12], but majorities of these models emphasize on the amplitude response, rather than on the phase response of the generated harmonics. Zheng and Coates [13] developed an analytical formula for the far-field angular response of the difference frequency wave, and evaluated the off-axis performance of parametric array. Subsequently, Zheng and Wang [14] proposed a numerical method, of which results are reported in close agreement with available experimental results within and beyond the Rayleigh distance of parametric array. However, the off-axis angle was limited to a small range due to the assumption that the parametric nonlinear interaction process in air was treated in a quasi-linear manner in both the above investigations.

Steering of directional sound beam is a useful feature for applications that require the parametric loudspeaker to steer to a targeted audience and not to disturb people nearby [15]. A direct approach is to turn the sound beam mechanically, as shown in Olszewski et al. [16]. However, mechanical structure is bulky and cannot be scaled down easily. Alternatively, a digital beamsteering approach for the parametric loudspeaker was proposed by Tan et al. [17], who exploited a group of bifrequency Gaussian sources but ignored the absorption effect in air. In their work, the delay-and-sum beamforming technique was

employed for electronically steering the primary beams so as to steer the audible beam towards the desired direction. The theoretical basis of this digital beamsteering method of the parametric loudspeaker can also be traced back to Darvennes and Hamilton [18]. They studied the difference frequency wave generated from two noncollinear Gaussian beams based on the nonlinear parabolic wave equation, and found that when restricted to moderate sources separations and interaction angles, the far-field directivity of the difference frequency wave is given by the product of the primary beam directivities. The product directivity principle was applied in the work of Gan et al. [19] on digital beamsteerers of the parametric loudspeaker, but they only provided simulation results of the proposed beamsteering algorithms and did not discuss the spatial aliasing issue.

In this paper, an equivalent Gaussian source array to the ultrasonic transducer array is proposed to prove the feasibility of devising a digital beamsteerer for the parametric loudspeaker. A new observation on the limitation of valid angle range for beamsteering, which is based on the nonlinear parabolic wave equation, is also stated for the parametric loudspeaker. Moreover, digital beamsteering approach of the parametric loudspeaker is carried out in experiment and links to the theoretical study. From the experimental measurements, we observe spatial aliasing of primary waves in the parametric loudspeaker and the formation of grating lobes of primary waves, which may or may not be completely inherited by the difference frequency wave, depending on the frequencies of the primary waves. This grating lobe elimination is also analyzed and verified through experiments.

This paper is organized as follows. In Section II, the beamforming structure of the parametric loudspeaker is given. In Section III, the grating lobe elimination of the parametric loudspeaker is observed and analyzed by simulations. The experiments of grating lobe elimination are carried out and discussed in Section IV. Lastly, Section V concludes this paper.

II. BEAMSTEERING STRUCTURE OF PARAMETRIC LOUDSPEAKER

One of the most popular model equations in nonlinear acoustics is the parabolic wave equation, also widely known as the Khokhlov-Zabolotskaya-Kuznetsov (KZK) equation [11], [12]. The KZK equation accurately describes the entire process of self-demodulation throughout the near-field and into the

far-field, for both on and off axis of the beam, and is expressed as follows:

$$\frac{\partial^2 p}{\partial z \partial \tau} = \frac{c_0}{2}\nabla_{\perp}^2 p + \frac{\delta}{2c_0^3}\frac{\partial^3 p}{\partial \tau^3} + \frac{\beta}{2\rho_0 c_0^3}\frac{\partial^2 p^2}{\partial \tau^2}, \tag{1}$$

where $\nabla_{\perp}^2$ is the Laplacian operator that operates in the plane perpendicular to the axis of the sound beam; p is the acoustic pressure; τ is the retarded time; δ is the diffusivity of sound; c_0 is the small-signal sound speed; β is the coefficient of nonlinearity; and ρ_0 is the ambient density. The effects of diffraction, absorption and nonlinearity in wave propagation are expressed by the first, second and third terms on the right hand side of (1), respectively.

There is however no general analytical solution to the KZK equation [20], but by considering acoustic sources with Gaussian amplitude shading, namely Gaussian sources, closed form solution can be found under the quasilinear approximation [9]. The source function q_1 of Gaussian sources is defined as

$$q_1(r) = p_0 \exp\left[-(r/a)^2\right], \tag{2}$$

where r is the distance to the center of the source; p_0 and a are the peak source pressure and the effective source radius, respectively.

Thus, the directivity function of Gaussian source can be derived from the linear solution component in the quasilinear approximation by substituting (2) into (1) [9]. The far-field Gaussian directivity D_G is given by

$$D_G(\theta) = \exp\left[-\frac{1}{4}(ka)^2 \tan^2\theta\right], \tag{3}$$

where θ is the angle (in degree) with respect to the axis of the beam, and k is the wavenumber. It is noted that from (3) that larger values of ka (*i.e.* larger ratios of source dimension to radiation wavelength) produce narrower beams. The variation of the Gaussian directivity with radiating frequency and effective radius is plotted in Fig. 1. Figure 1(a) shows that when the radiation frequency increases from 30 kHz to 50 kHz and the effective radius of the Gaussian source is fixed at 8 mm, the beamwidth decreases. Figure 1(b) shows another case when the radiation frequency is fixed and the effective radius of the Gaussian source varies from 2 mm, 5 mm to 8 mm. It is observed that the Gaussian directivity gets shaper with

higher operating frequency and smaller source radius.

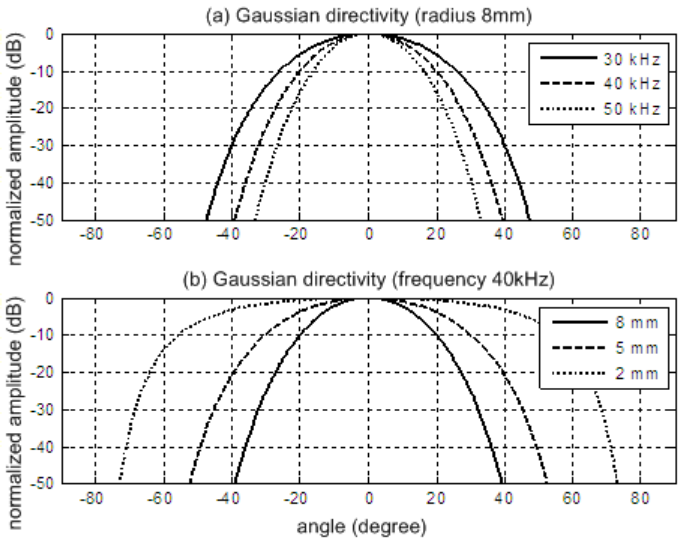

Fig. 1. Gaussian directivity varying with (a) the radiation frequency and (b) the effective radius.

When considering the difference frequency wave due to the radiation from a bifrequency Gaussian source, the difference frequency wave is given by the product of the directivities of the two primary frequency waves in the far-field, which is known as the product directivity principle [18]. However, the ultrasonic transducer array in the parametric loudspeaker [15]-[17] is usually separately weighted and equally spaced, and all the transducers in the linear array are assumed omnidirectional instead of Gaussian sources. Typical beampattern of 8-channel uniform linear transducer array with half wavelength spacing and using Chebyshev weights that achieve a sidelobe level of 20 dB is shown in Fig. 2(a). In practice, either a single transducer or a group of transducers are driven by the same output from each channel of the transducer array. Channel directivity is considered as the directivity pattern transmitted from one channel of the transducer array. Due to the channel directivity, the heights of sidelobes are reduced and no longer equal. The beampattern of the 8-channel transducer array is only plotted from -40˚ to 40˚ in Fig. 2(b) in accordance with the half power beamwidth of the channel directivity. Note that each lobe in the beampattern of a uniform linear transducer array has a bell shape similar to the directivity of a single Gaussian source. Thus, a transformation can be proposed to obtain an equivalent Gaussian source array from a linear uniform transducer array whose beampattern is given. In a seminal paper, Wen and

Breazeale [21] demonstrated that it was possible to accurately simulate the sound beam of a piston source by the superposition of ten Gaussian beams. They obtained the coefficients by fitting the Gaussian sources to match the piston velocity distribution on the surface of the transducer using a nonlinear least squares approach. A similar idea is used here. Each Gaussian source in the equivalent array is assigned an effective radius and an angular offset. Thus, each Gaussian source can represent one lobe in the beampattern plot. The directivity patterns of the Gaussian source arrays, which are equivalent to Figs. 2(a) -(b), are plotted in Figs. 2(c)-(d), respectively. Two kinds of mismatches are observed between the equivalent Gaussian source array and the transducer array in Figs 2(e)-(f). First, the sidelobes in the beampattern plot of the transducer array become more asymmetric when the incidence angle becomes larger. The asymmetric sidelobes result as peaks in the mismatch beampatterns. Second, the mismatches between the equivalent Gaussian source array and the transducer array becomes larger at the gaps between two sidelobes. Through the mismatches at the gaps are obvious, they occupy relatively small ranges of incidence angle. Fig. 2 illustrates that when the overall directivity of the transducer array is given by multiplying its theoretical beampattern with the channel directivity, the nonlinear least square approach can still work out an equivalent Gaussian source array that match the overall beampattern of the transducer array well.

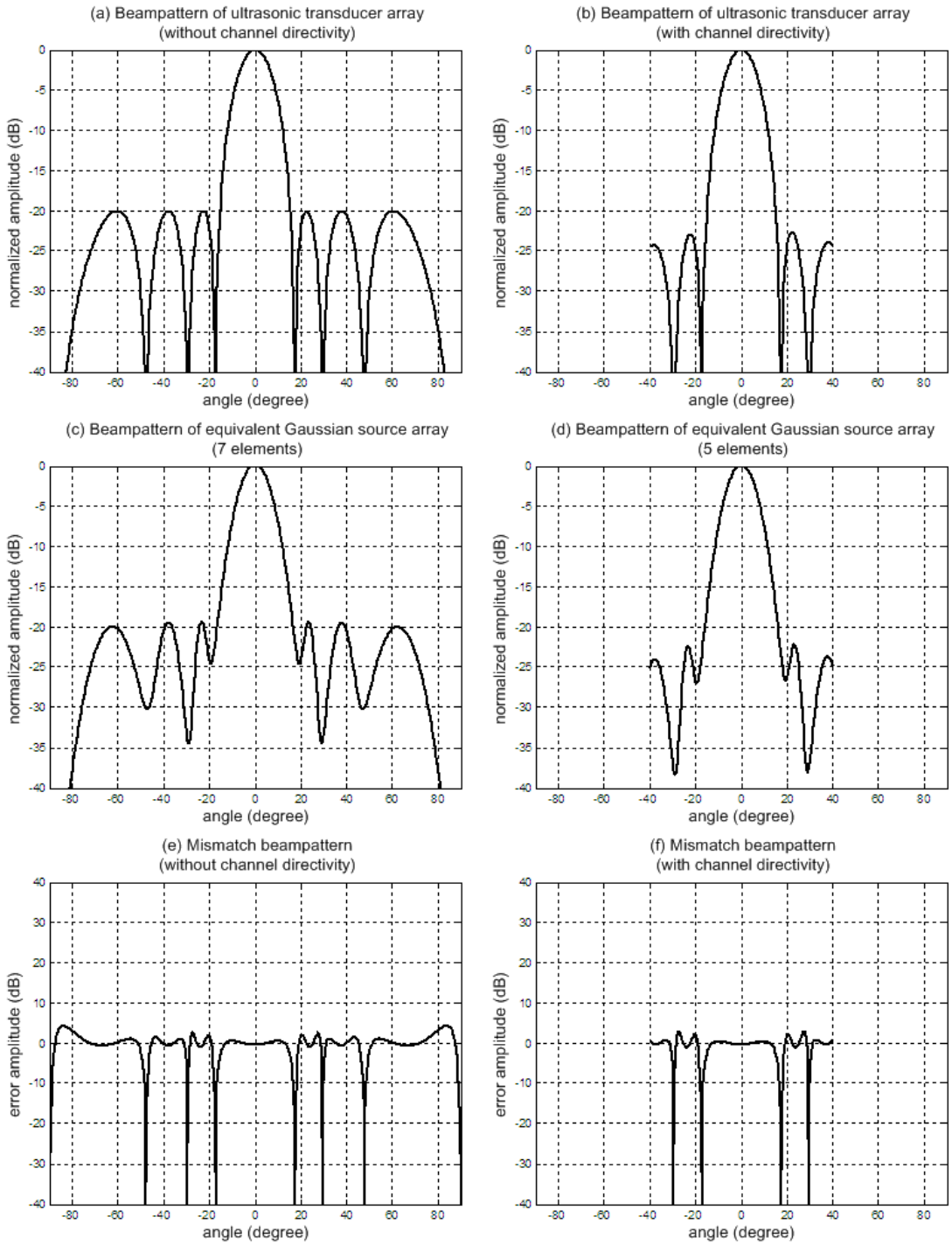

Fig. 2. (a) Beampattern of a transducer array (8 channels) with Chebyshev weights giving 20 dB sidelobe level when the spacing is half the wavelength; (b) beampattern of a transducer array (8 channels) with Chebyshev weights giving 20 dB sidelobe level taking into account of the channel directivity; (c) beampattern of the equivalent Gaussian source array (7 elements) to (a); (d) beampattern of the equivalent Gaussian source array (5 elements) to (b); (e) mismatch beampattern between (a) and (c), which excludes the channel directivity; (f) mismatch beampattern between (b) and (d), which includes the channel directivity.

The equivalent circular Gaussian source array can provide a novel observation of the validation of

the product directivity principle. For example, a uniform linear transducer array with half wavelength spacing is shown in Fig. 3(a). There are 7 lobes in this beampattern plot, so the same number of Gaussian sources is required to achieve a good match between the transducer array and the circular Gaussian source array, as illustrated in Fig. 3(b). The Gaussian sources in the equivalent circular array are different sizes according to the beamwidths of distinguish lobes, and are placed at the angular peaks' locations of the corresponding lobes. Therefore, by choosing the effective radius for each Gaussian source, as shown in Fig. 3(b), the directivity of Gaussian source can fit the shape of lobes when the radiating frequency is fixed.

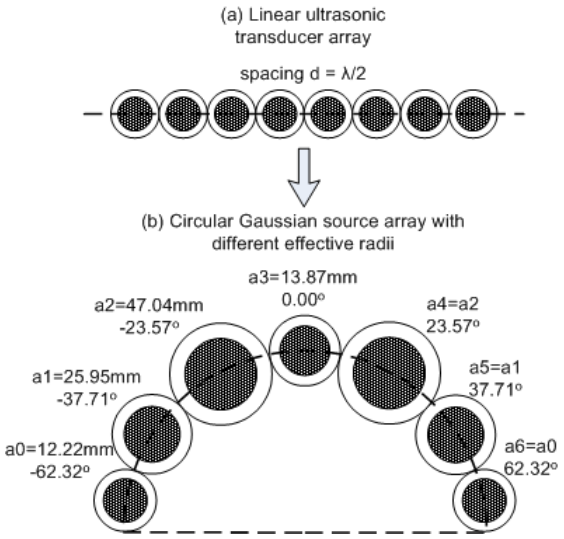

Fig. 3. (a) A uniform linear transducer array (8 elements, half wavelength spacing) is transformed into (b) an equivalent circular Gaussian source array (7 elements), where a_i (i = 0,1,2,…,6) shows the effective radius of each Gaussian source located at the indicated angle.

Since the product directivity principle is derived from the parabolic wave equation that is only valid in the vicinity of the propagating axis, the range of valid angle is limited within an angle of ±15˚ as a result of constraint imposed by the KZK equation [9]. In particular, when the ultrasonic transducers in the linear array are assumed Gaussian sources, their propagation axes are parallel. Therefore, the range of valid angle of the whole transducer array is still limited within an angle of ±15˚. But when the uniform linear transducer array is considered as equivalent to a circular Gaussian source array, the propagating axes of Gaussian sources are distributed. Thus, the range of valid angle of the circular Gaussian source array is given by the union of the ranges of valid angles of all the Gaussian sources. In this sense, the

product directivity principle can always be applied to the parametric loudspeaker.

According to the product directivity principle, the directivity of the difference frequency wave can be adjusted by controlling the directivity of the primary waves. Figure 4 shows a simplified structure of a beamsteerer used in the parametric loudspeaker, where the total number of channels is denoted as M. Assume that the ultrasonic transducer array is steered in the same direction and shares the same group of weights for two primary frequency waves. Therefore, the difference frequency wave is also steered to that direction, and the far-field beampattern of the steered ultrasonic transducer array for the primary frequency wave is given by

$$H(k,\theta)=\left|\sum_{m=0}^{M-1} w_m \exp\left\{ jmdk\left(\sin\theta-\sin\theta_0\right)\right\}\right|, \tag{4}$$

where w_m are the weights of channels for m = 0,1,2,..,M –1; the output of each channel can drive a group of transducers which are configured into different shapes; d is the spacing between channels in the ultrasonic transducer array; k is the wavenumber of the transmitted primary frequency wave; θ is the incidence angle that can range from -90˚ to 90˚; and θ_0 is the steering angle of the ultrasonic transducer array.

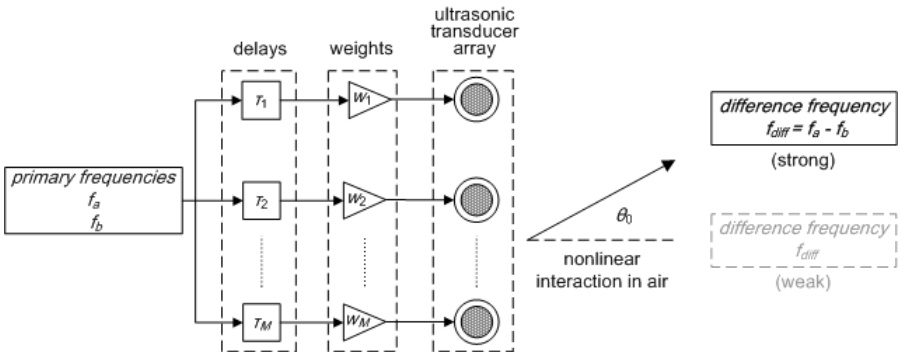

Fig. 4. Beamsteering structure of the parametric loudspeaker.

Based on the product directivity principle, the far-field directivity of the difference frequency wave $D_{diff}(\theta)$ is given by

$$D_{diff}(\theta)=H(k_a,\theta)H(k_b,\theta), \tag{5}$$

where k_a and k_b are the wavenumbers of primary frequencies f_a and f_b, respectively. We always assume

that $f_a < f_b$ without lost of generality. Thus, the difference frequency wave generated from the two primary frequency waves is given by $f_{diff} = f_b - f_a$.

For simplicity, the product directivity can be defined as

$$D_{diff}(\Lambda, F, \Theta) = H(k_a, \theta) H(k_b, \theta) = \left| \sum_{m=0}^{M-1} w_m \exp\left(j2\pi m \frac{\Theta}{\Lambda} \right) \right| \cdot \left| \sum_{m=0}^{M-1} w_m \exp\left(j2\pi m \frac{\Theta}{\Lambda} F \right) \right|, \quad (6)$$

where Λ is the ratio of the wavelength of the lower primary frequency f_a to the spacing of the ultrasonic transducer array, given by $\Lambda = \lambda_a / d$; F is the ratio of the higher primary frequency to the lower primary frequency, given by $F = f_b / f_a$; and Θ is the normalized angle, given by $\Theta = \sin\theta - \sin\theta_0$.

III. GRATING LOBE ELIMINATION OF PARAMETRIC LOUDSPEAKER

Typical ultrasonic transducer [22] with a resonance frequency of 40 kHz has a diameter of less than 16 mm. However, the primary wavelength for the 40 kHz signal is less than 8.5 mm, which is much smaller than the diameter of the ultrasonic transducer. Though it is not surprise to observe spatial aliasing of primary frequency waves in the parametric loudspeaker, certain grating lobes of primary frequency waves are not completely inherited by the difference frequency wave. This grating lobe elimination can occur only under some conditions for the difference frequency wave in the parametric loudspeaker. To help analyze the prerequisites on the grating lobe elimination, it is assumed that the weights used in the beamsteering structure of the parametric loudspeaker are symmetric with reference to the center channel, and the steering angle is chosen between $0° \leq \theta_0 \leq 90°$, without lost of generality.

The angular distances between grating lobes of primary frequency waves is helpful to quantify the level of grating lobe eliminations. For example, the grating lobe elimination of the difference frequency wave can be achieved when the angular distance between grating lobes of primary frequency waves are far apart. The direction where grating lobes occur can be found at $\Theta_a = n_a \Lambda$ for the lower primary frequency f_a and $\Theta_b = n_b \Lambda / F$ for the higher primary frequency f_b, where n_a and n_b are indices of grating lobes. The distance function, which describes the minimum angular distance between grating lobes of two primary frequency waves, is defined as

$$D_K(F) = \min_{\substack{0 \le n_a \le K \\ 0 \le n_b \le L}} \left(\left| n_a \Lambda - \frac{n_b \Lambda}{F} \right| \right), \tag{7}$$

where K is the largest index of grating lobe of the lower primary frequency f_a in the visible region where the incidence angle is between $\pm 90°$; L is the largest index of grating lobe of the higher primary frequency f_b in the visible region. Because $f_a < f_b$ is assumed, K must be less than L, and $F > 1$. Furthermore, to compute the values of the distance function, K needs to be assigned in advance.

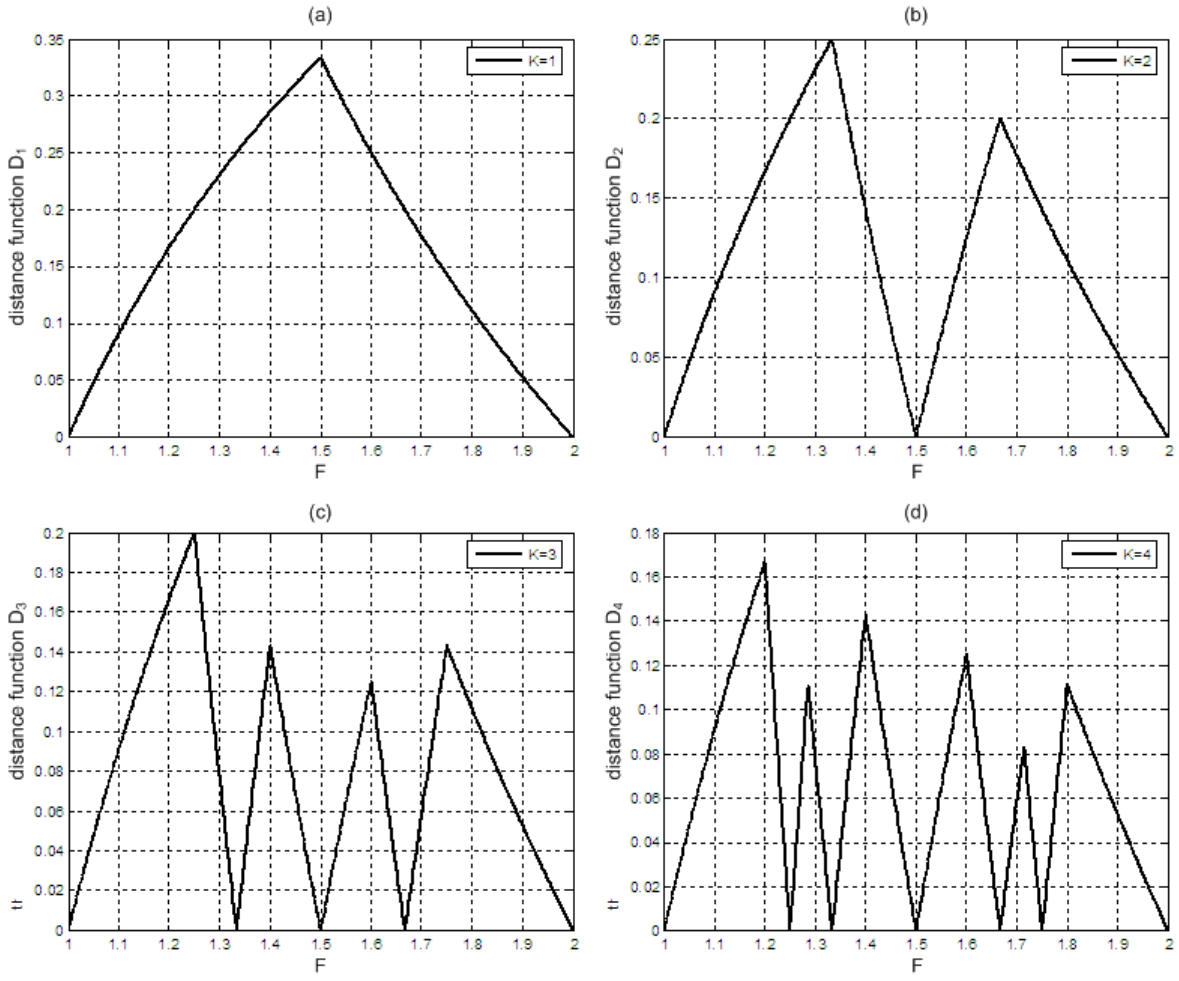

Fig. 5. Distance function when considering (a) K =1, (b) K =2, (c) K =3, and (d) K =4 grating lobes.

Figure 5 shows the distance function when K = 1,2,3,4 and $1 < F < 2$. Nulls in the distance function show the occurrence of grating lobes for difference frequency wave. When two grating lobes of primary frequency waves arise in the same direction, the value of distance function reduces to 0. This observation can be shown in Fig. 6(a) when the second grating lobe of 40 kHz primary wave coincides with the third

grating lobe of 60 kHz primary wave. Therefore, nulls in the distance function constrain the range of F that must be chosen between two neighboring nulls to prevent grating lobes of the difference frequency wave. To ensure the ability of generating low difference frequency, the null where F =1 must be chosen as the lower bound of the valid range of F. From (7), nulls in the distance function are located where $F = n_b / n_a$. Setting $n_a = K$ and $n_b = K + 1$ gives the upper bound of the valid range of F, which represents the null that is closest to 1. Thus, the upper bond of F is given by $F = (K + 1) / K$. Note that the location of nulls in distance function is not related to the estimation of L. So the range of F, given by $1 < F < 1 + 1 / K$, is valid whenever K is assigned.

The difference frequency is generated from the two primary frequency waves, given by $f_{diff} = f_b - f_a$. Derived from the definition of F, $f_{diff} / f_a = F - 1$. Therefore, the range of the difference frequency is given by $0 < f_{diff} < f_a / K$. If the parametric loudspeaker is designed to generate all the audible frequencies below 20 kHz, K should be less than f_a / 20 kHz. In practice, f_a is normally chosen to be around 40 kHz (*i.e.* coincide with the resonating frequency of the typical ultrasonic transducer [22]). Therefore, it is reasonable to assign K =2.

The relation between steering angle and the number of grating lobes of primary frequency waves can be found in the Nyquist criterion [23], the range of Λ is approximately given by

$$\Lambda = \frac{\lambda_a}{d} \geq \frac{1+\sin\varphi}{(K+1)}, \tag{8}$$

where φ is the maximum steering angle. For example, setting K = 2, φ = 90 °, the spacing of the ultrasonic transducer array d is found to be less than one and half the wavelength. In the case of using upper single sideband modulation and the carrier frequency (*i.e.* f_a) is 40 kHz, the maximum non-aliasing spacing of the ultrasonic transducer array is 12.75 mm. In another beamsteering example of K = 2, φ = 30 °, the largest spacing can achieve two times wavelength of the lower primary frequency wave to prevent grating lobes at the difference frequency. Therefore, the non-aliasing spacing of the ultrasonic transducer array can now be widened to 17 mm.

As discussed above, the grating lobes of the difference frequency wave appear where there are nulls in the distance function. In addition, grating lobes are suppressed within the vicinity of nulls in the distance function due to the product directivity principle. Thus, intersection function is proposed to describe the elimination of grating lobes of the difference frequency wave when the distance between grating lobes of primary frequency waves is given by the distance function. Intersection function is defined as

$$I_K(F) = \max_{\Theta}\left\{\left|\sum_{m=0}^{M-1} w_m \exp\left(j\pi m\frac{\Theta}{\Lambda}\right)\right| \cdot \left|\sum_{m=0}^{M-1} w_m \exp\left[j\pi m\frac{F}{\Lambda}\left(\Theta - D_K(F)\right)\right]\right|\right\}. \quad (9)$$

Based on the beamsteering structure in Fig. 4, simulations are carrier out for an ultrasonic transducer array with 16 channels. The spacing d is chosen as twice the wavelength of the lower primary frequency wave (*i.e.* $\beta = 2$ and $f_a = 40$ kHz). The higher primary frequency f_b is selected as 60 kHz, 50 kHz, 42 kHz, resulting in $F = 1.5$, 1.25, 1.05, respectively. The steering angle θ_0 is specified as 15˚, and w_m are chosen as Chebyshev weights with 30dB attenuation. The simulated beam patterns for three sideband frequencies are plotted in their respective plots of Figs. 6(a)-(c). Grating lobes (1,2,3,…) in the figures are indexed from right to left, and the mainlobe is labeled as 0.

In Fig. 6(a), the second grating lobe of the lower primary frequency (f_a = 40 kHz) only coincides with the third grating lobe of the higher primary frequency (f_b = 60 kHz). In this case, spatial aliasing of the difference frequency (f_{diff} = 20 kHz) occurs at -50˚. In Fig. 6(b), grating lobes of the lower primary frequency (f_a = 40 kHz) coincide with sidelobes of the higher primary frequency (f_b = 50 kHz) that result in sidelobes of the difference frequency (f_{diff} = 10 kHz). Heights of all the sidelobes in the difference frequency wave are not higher than the highest sidelobe of primary frequency waves. This case is called the grating lobe elimination. In Fig. 6(c), the first grating lobe of the lower primary frequency (f_a = 40 kHz) appears in the direction close to the first grating lobe of the higher primary frequency (f_b = 44 kHz). Two grating lobes that are closely spaced result in a sidelobe at the difference frequency (f_{diff} = 4 kHz) that is lower than the mainlobe but higher than the highest sidelobe of primary frequency waves. This case is considered as a partial eliminated grating lobe of primary frequencies. The intersection function

for this group of simulations is plotted in Fig. 6(d). The grey bar at the bottom of Fig. 6(d) shows the region of partial grating lobe elimination, and the black bar illustrates the region of grating lobe elimination.

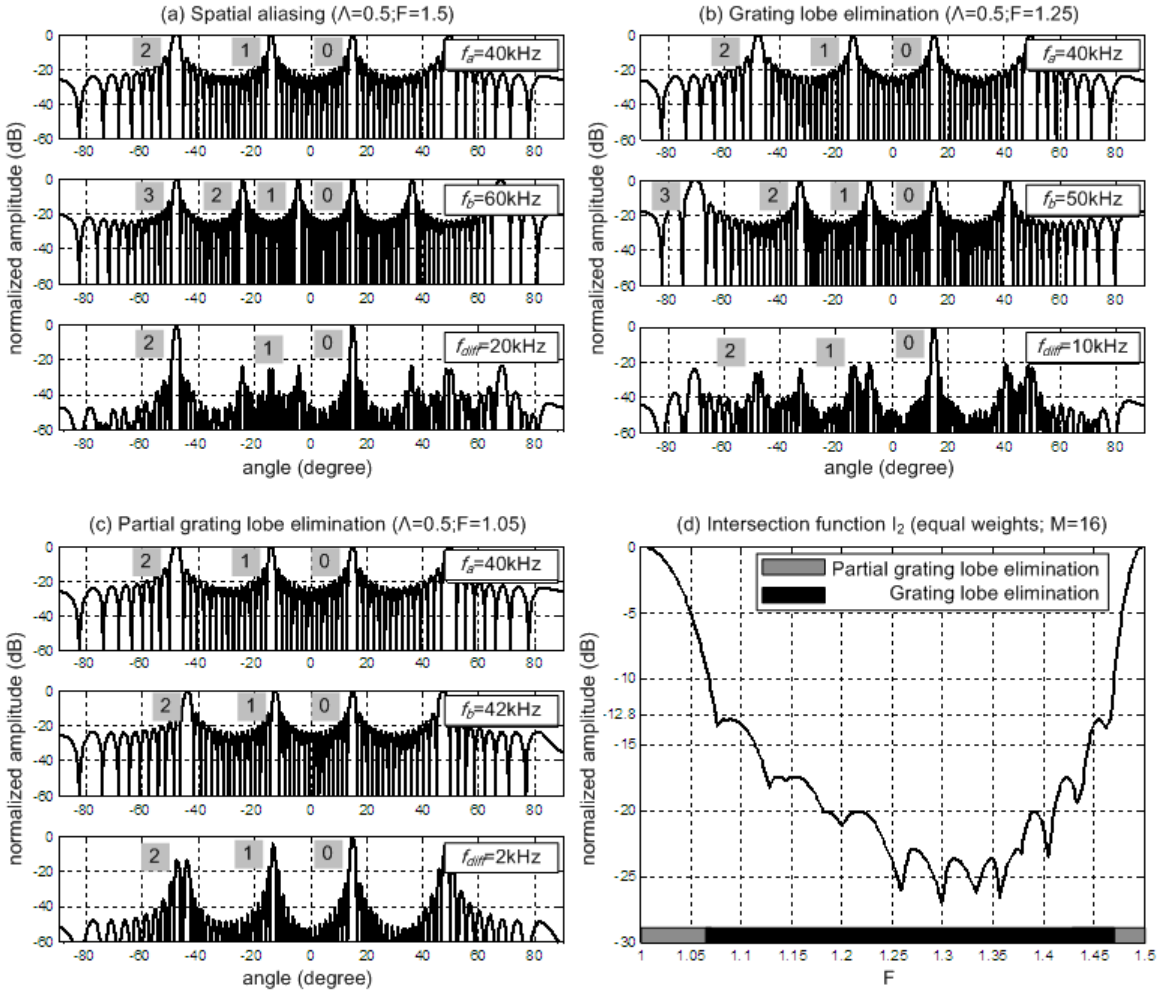

Fig. 6. Three cases, (a) spatial aliasing, (b) grating lobe elimination, and (c) partial grating lobe elimination occur in an ultrasonic transducer array with 16 channels (M =16) and twice the wavelength spacing (Λ=0.5). The intersection function for this array configuration and equal weights is plotted in (d) to show the ranges of F that lead to different cases.

In another scenario, the spacing d is changed to one and a half times the wavelength of the lower primary frequency (*i.e.* β = 1.5). The number of channels and the lower primary frequency are kept at 8 and 40 kHz, respectively. The higher primary frequency is selected as 60 kHz, 50 kHz, 44 kHz, resulting in F = 1.5,1.25,1.1, respectively. The steering angle θ_0 is specified at 35˚, and w_m are chosen as equal weights. Spatial aliasing, grating lobe elimination and partial grating lobe elimination cases are shown by

Figs. 7(a)-(c), respectively. The intersection function for this group of simulations is plotted in Fig. 7(d). The grey bar at the bottom of Fig. 7(d) shows the region of partial grating lobe elimination, and the black bar illustrates the region of grating lobe elimination.

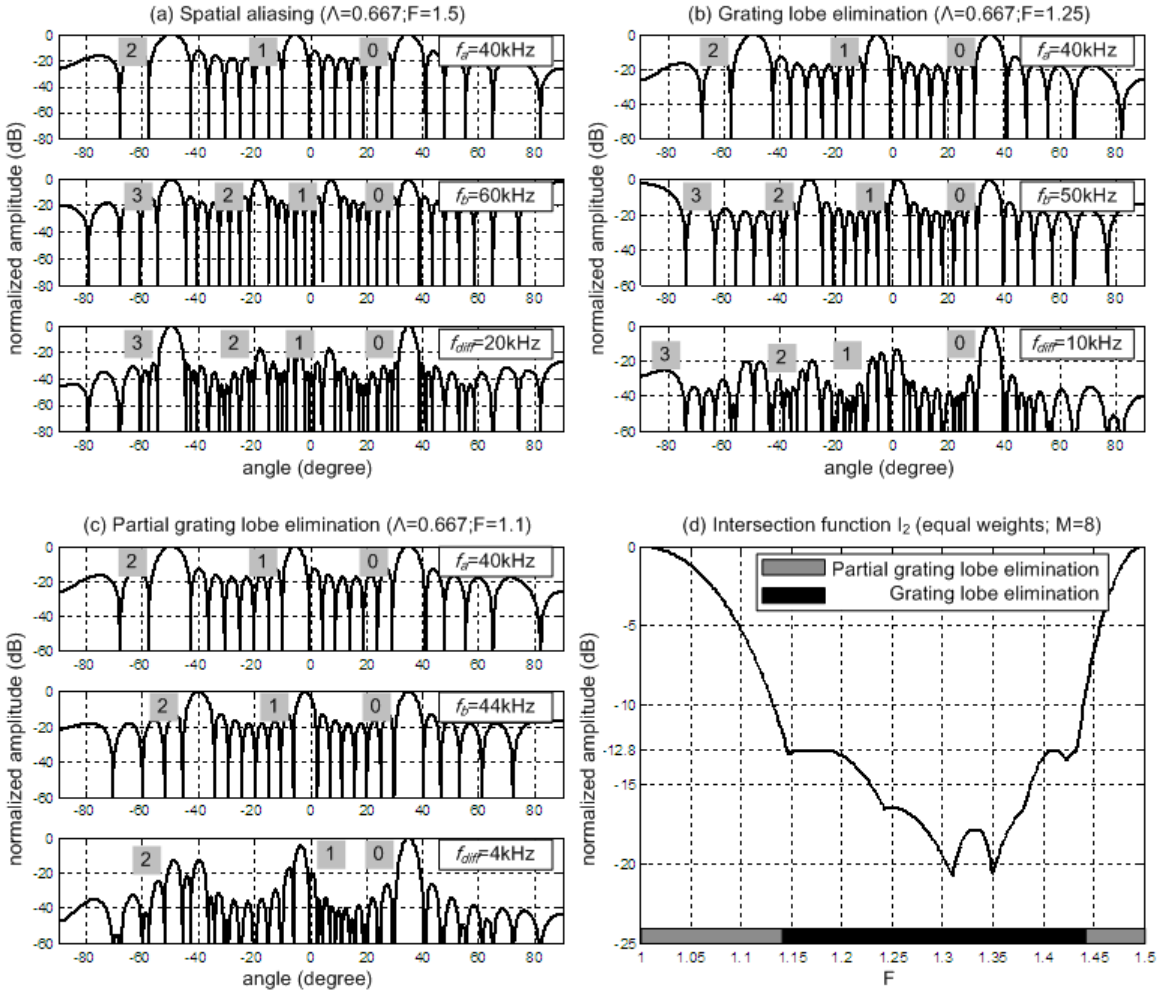

Fig. 7. Three cases, (a) spatial aliasing, (b) grating lobe elimination, and (c) partial grating lobe elimination occur in a ultrasonic transducer array with 8 channels (M =8). The spacing is one and a half the wavelength (Λ=0.667). The intersection function for this array configuration and equal weights is plotted in (d) to show the ranges of F that lead to different cases.

When the transducer spacing is reduced from $2\lambda_a$ (in Fig. 6) to $1.5\lambda_a$ (in Fig. 7), the number of grating lobes in the beampattern plots of primary frequency waves is reduced due to insufficient spatial sampling rate. However, the largest index of grating lobes at the lower primary frequency is constant as K =2, because the steering angle also changes from 15˚ to 35˚, as stated in (8).

In Figs. 8(a)-(b), we set $K = 2$, $1 < F < 1.5$, and the number of channels $M = 8$. The spacing of the ultrasonic transducer array used to plot Figs. 8(a)-(b) are $1.5\lambda_a$ and $2\lambda_a$, respectively. Slight differences are observed between curves of intersection functions. However, these differences are found not to affect the ranges of F that ensure the grating lobe elimination, since the changed segments are subsets of the ranges of F that ensures the grating lobe elimination. Note that from the definition of the intersection function, it can also be discovered that the range of F that ensures the grating lobe elimination is not changed with Λ. (see appendix for detail explanation).However, the value of Λ can affect the occurrence of grating lobe elimination in an implicit way. In practice, closer spacing between channels in the ultrasonic transducer array leads to less grating lobes. The value of Λ in (8) determines the number of grating lobes of the lower primary frequency wave.

In Fig. 8(c), K is set to 1. Within the range of $1 < F < 1.5$, we can only obtain the lower bound of F which ensures the grating lobe elimination, since the upper bound has already been beyond the range of F that we are considering. Correspondingly in Fig. 5(a), the distance function when K =1 has only one null within the range $1 < F < 1.5$.

Another factor that determines the grating lobe elimination is the number of channels used in the ultrasonic transducer array. In Fig. 8(d), the number of channels M is increased to 16. Comparison between Fig. 8(a) and Fig. 8(d) shows that the number of channels can significantly affect the range of grating lobe elimination. Another advantage of increasing number of channels is obtaining narrower beams, but this is traded off by using more digital-to-analog convertors and processing complexity.

Through the comparison among all the four subplots of Fig. 8, beamsteerer using Chebyshev weights with 20 dB attenuation results in comparable range of F compared to beamsteerer using equal weights. Chebyshev weights with 10 dB and 30 dB attenuation result in the widest and narrowest range of F, respectively. In order to achieve higher attenuation, the range of difference frequency is sacrificed. Once the range of F is fixed, increasing the carrier frequency widens the range of difference frequency generated from the parametric loudspeakers. However, the bound of F is proportional to the bound of the difference frequency in parametric loudspeakers. Increasing carrier frequency increases both the lower

and upper bounds of the difference frequency. Therefore, a better way to build the ultrasonic transducer array in the parametric loudspeaker is to increase the number of channels, which widens the ranges of F and the difference frequency, and preserves the ability of generating low frequency as well.

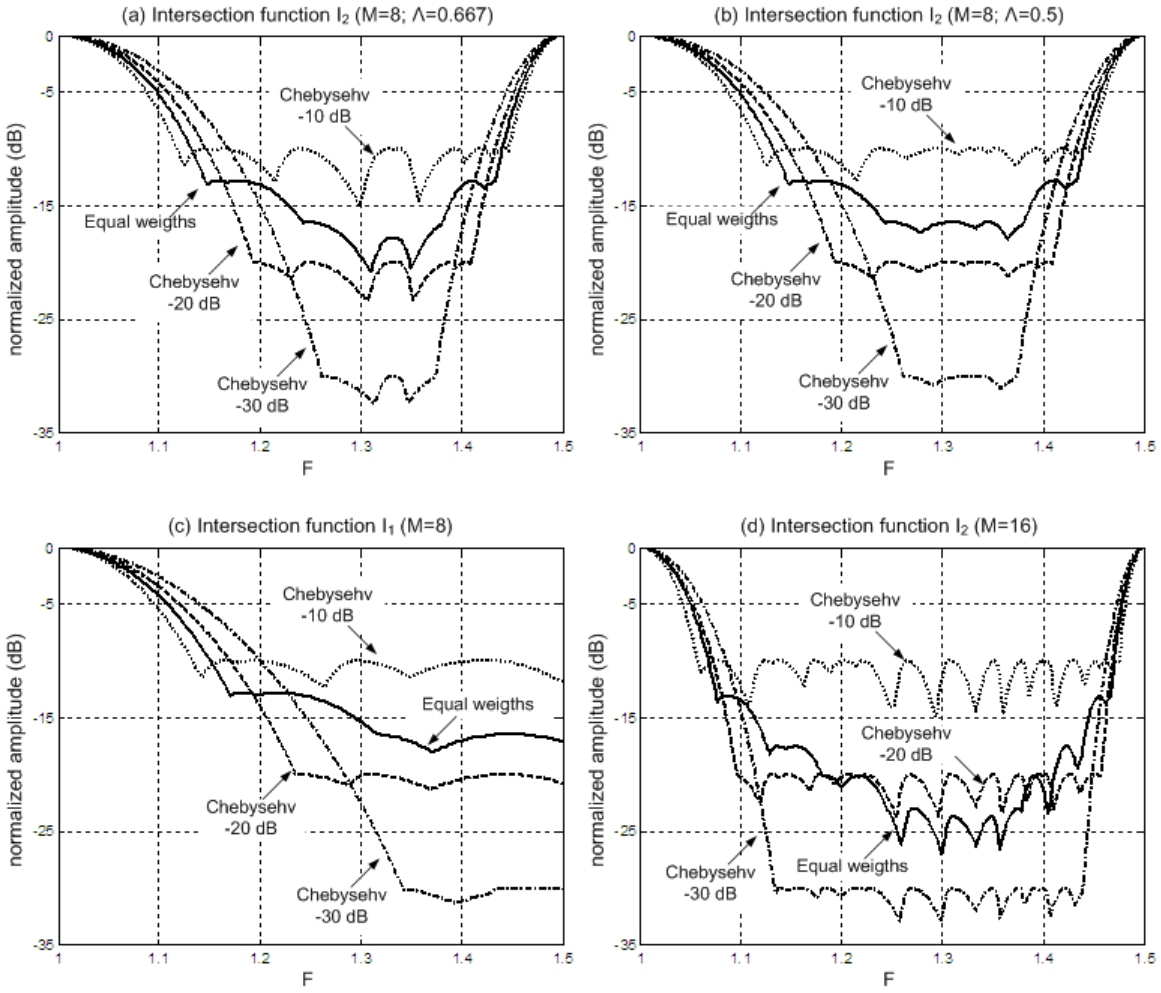

Fig. 8. Intersection function with four groups of weights (equal weights and Chebyshev weights with 10 dB, 20 dB, 30 dB attenuations): (a) 8 channels, one and a half wavelength spacing, and appearance of two grating lobes for the lower primary frequency wave; (a) 8 channels, two times wavelength spacing, and appearance of two grating lobes for the lower primary frequency wave; (c) 8 channels, half wavelength spacing, and appearance of only one grating lobes for the lower primary frequency wave; (d) 16 channels, half wavelength spacing, and appearance of two grating lobes for the lower primary frequency wave.

IV. EXPERIMENT RESULTS

Grating lobes appear in the beampattern of primary frequency waves when the spacing of channels is larger than half the wavelength of primary frequency waves in the ultrasonic transducer array. This is commonly known as the Nyquist criterion [24] in array signal processing theory. However, the simulation

results reveal that the Nyquist criterion is no longer applied to the difference frequency wave generated by the parametric loudspeaker. When the primary waves are steered to the same direction, their mainlobes coincide with each other. But because of the difference between wavenumbers of the two primary waves, the spatial aliasing periods for the two primary waves are also different. Thus, the grating lobes of two primary frequency waves do not coincide at the same direction all the times. It allows the grating lobes of primary frequency waves to suppress each other at the difference frequency wave based on product directivity principle. The spacing limitation has been relaxed to ensure sufficient spatial sampling rate at the difference frequency in parametric loudspeakers.

In this section, we conduct experimental measurement to determine the grating lobe elimination of the difference frequency wave in cases described in the previous sections. The experiment was conducted in an anechoic chamber with a dimension of 6 m$\times$3 m$\times$3 m. Primary frequency waves were captured by an 1/8 inch microphone (B&K 4138), and the difference frequency wave was measured by a 1/2 inch microphone (B&K 4134). The ultrasonic transducer array was mounted on a motorized rotary stage, and the microphones were placed at a location 4 meters away from the center of the ultrasonic transducer array, as shown in Fig. 9. The beamwidth of the Murata ultrasonic transducer (MA40S4S) [22] used in our experiments is stated as 80˚ in the data specification. Therefore, the beampatterns of the difference frequency wave, as well as the primary frequency waves were restricted to be measured from -40˚ to 40˚ with a resolution of 1˚. The sound was estimated to propagate at 343 m/s in air. All the channels in the ultrasonic transducer array were equally weighted, but differently delayed to achieve beamsteering. The beamsteering structure shown in Fig. 4 was implemented in a data acquisition board (NI PCI-6733).

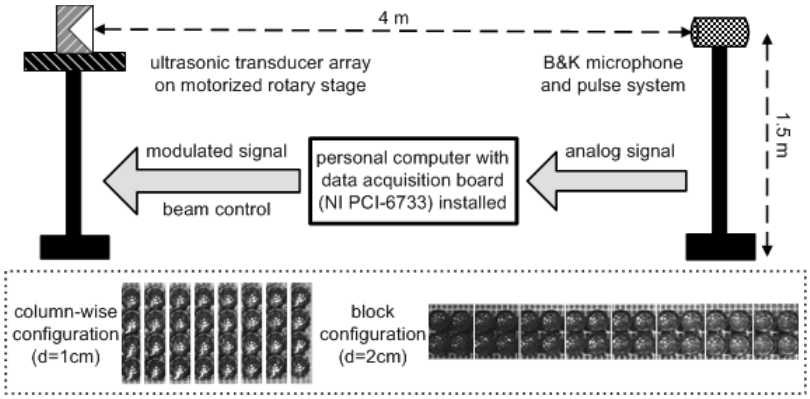

Fig. 9. The configuration of the transducer array and the microphones used in the experiments.

The experiments were first carried out using column-wise configuration with spacing of d = 1 cm. The output of each channel drives four transducers in a column, and the channel directivity is shown in Fig. 10(a). Each channel is considered as a transducer unit in the beamsteering structure shown in Fig. 4. The steering angle of primary frequency waves was fixed at -20˚, and the primary frequencies were adjusted to achieve three difference frequencies of 8 kHz, 4 kHz and 1 kHz. In order to compare the measurement results with the simulation results reported in the previous sections, we use (4) to compute the beampattern with the contribution of channel directivity for the two primary frequency waves. However, in the simulation result for the difference frequency wave, two simulation approaches can be derived by either using the product of simulated beampatterns of primary frequency waves as well as the channel directivities (stated as Simulation I), or using the product of measured beampatterns of primary frequency waves (stated as Simulation II). The experimental results as well as the corresponding simulation results are shown in Fig. 11.

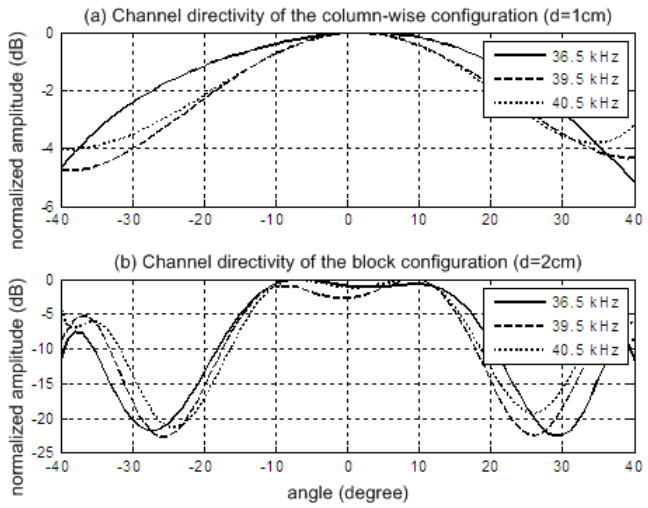

Fig. 10. (a) Measured channel directivity of the column-wise configuration; (b) Measured channel directivity of the block configuration.

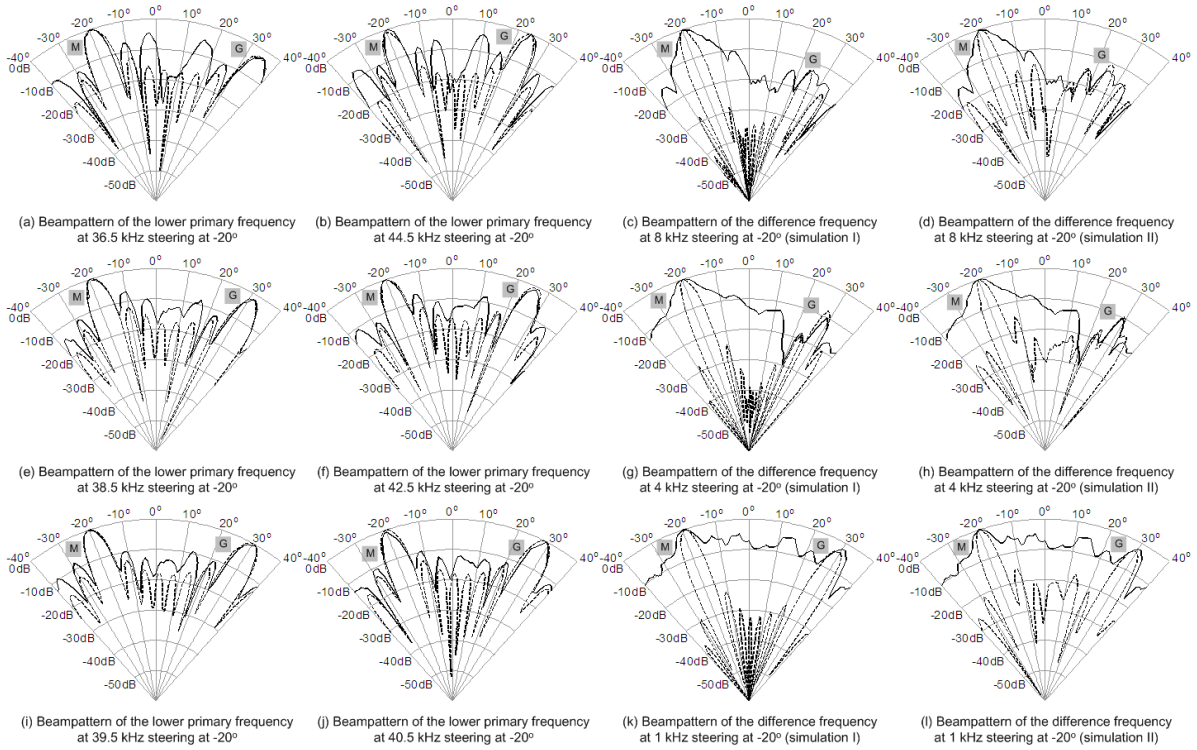

Fig. 11. Experimental results and simulation results using column-wise configuration (M: mainlobe; G: grating lobe) are plotted in solid lines and dash lines, respectively. (a)-(d) show beampatterns of primary frequencies (36.5 kHz and 44.5 kHz) and difference frequency (8 kHz), and illustrate a case of grating lobe elimination; (e)-(h) show beampatterns of primary frequencies (38.5 kHz and 42.5 kHz) and difference frequency (4 kHz), and illustrate a case of partial grating lobe elimination; (i)-(l) show beampatterns of primary frequencies (39.5 kHz and 40.5 kHz) and difference frequency (1 kHz), and illustrate a case of spatial aliasing at the difference frequency.

Mainlobes of both primary frequencies and difference frequencies are marked as 'M' in Fig. 11. Grating lobes of the primary frequencies, as well as the eliminated grating lobes of the difference

frequencies, are marked as ‘G’ in Fig. 11. Figs. 11(a)-(d) show a case of grating lobe elimination. The results are obtained when the primary frequencies are given by 36.5 kHz and 44.5 kHz, and the generated difference frequency is 8 kHz. The grating lobes are located at 35˚ and 24˚ in the beampatterns of 36.5 kHz and 44.5 kHz primary waves, respectively in Figs. 11(a)-(b). For the higher primary frequency beampattern (in Fig. 11(b)), the grating lobe is closer to the mainlobe compared to the lower primary frequency beampattern. Because of sufficient angular distance between the two grating lobes, grating lobe elimination occurs in the difference frequency wave. The highest sidelobe that is an eliminated grating lobe is located at 25˚ in Figs. 11(c)-(d). Figure 11(c) shows the result of simulation I, which can predict the height of eliminated grating lobe based on the simulated beam patterns of the primary frequency waves; while Fig. 11(d), which represents the case for Simulation II, shows a better match between the experimental result and the simulation result. A case of partial grating lobe elimination is shown in Figs. 11(e)-(h). The primary frequencies are chosen as 38.5 kHz and 42.5 kHz, and the generated difference frequency is 4 kHz. The grating lobes are located at 31˚ and 26˚ in the beampatterns of 36.5 kHz and 44.5 kHz primary waves, respectively, shown in Figs. 11(e)-(f). These two grating lobes are still apart from each other, but result in partial grating lobe elimination due to the smaller angular distance between them. The partial eliminated grating lobe is located at 29˚ in Figs. 11(g)-(h). The simulated beam patterns in the cases of simulation I and II generates two similar results for both mainlobe and partial eliminated grating lobe. The last set of results shows a case of spatial aliasing, as illustrated in Figs. 11(i)-(l). The primary frequencies are given by 39.5 kHz and 40.5 kHz. Thus, the difference frequency is 1 kHz. Both the grating lobes are located at 30˚ in the beampatterns of 39.5 kHz and 40.5 kHz primary waves, shown in Figs. 11(i)-(j). These two grating lobes result in spatial aliasing because they are located too close to each other. The grating lobe of the difference frequency wave is slightly lower than the mainlobe due to the channel directivity of the ultrasonic transducer array (see Figs. 11(k)-(l)). Both results of simulation I and simulation II can match the measured beampattern of the difference frequency wave at the vicinity of mainlobe and grating lobe. However, for the other angles, simulation II matches better to the experimental result compared to simulation I.

From the above experimental results, when the difference frequency increase, the grating lobes of the two primary frequency waves become further apart in angular distance and full or partial grating lobe elimination can occur. However, when the difference frequency gets smaller, spatial aliasing become a problem. These experiments also verified that the product directivity principle can be used to predict the directivity of the delay-and-sum structure for the parametric loudspeaker.

The next experiment looks into a different configuration, known as the block configuration. In our experiment, four ultrasonic transducers are grouped into a single channel with a spacing of $d = 2cm$ between the centroid of neighboring channels. The directivity pattern for the primary frequency waves of the block configuration plotted in Fig. 10(b) has two sidelobes and two dips located around ±25˚. Due to the sharper directivity pattern of the block configuration, the steering angle can only be selected within ±15˚. Outside these angles, the mainlobe of the transducer array is greatly suppressed. The experimental results, as well as the corresponding simulation results, are shown in Fig. 12.

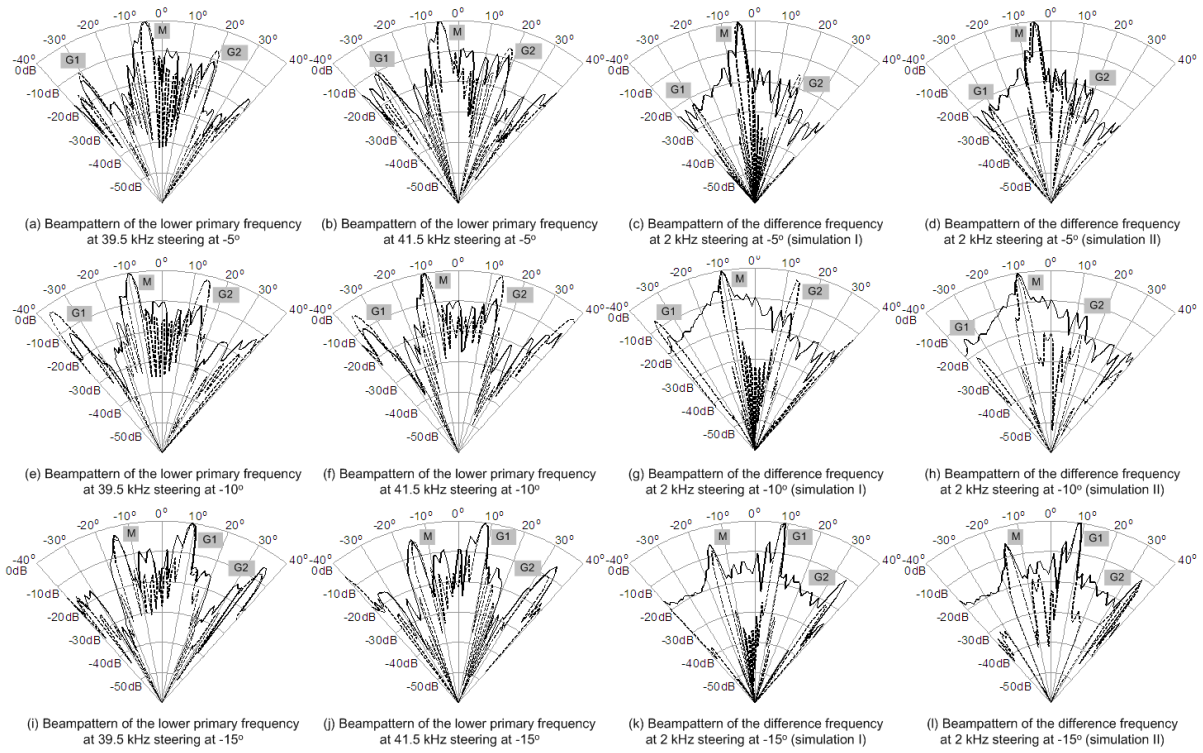

Fig. 12. Experimental results and simulation results using block configuration (M: mainlobe; G1 and G2: grating lobe) are plotted in solid lines and dash lines, respectively. The primary frequencies are 39.5 kHz and 41.5 kHz, and the difference frequency is 2 kHz. (a)-(d) show a case of grating lobe elimination when the primary frequencies are steered to -5˚; (e)-(h) show a case of partial grating lobe elimination when the primary frequencies are steered to -10˚; (i)-(l) show a case of spatial aliasing when the primary frequencies are steered to -15˚.

Similar to the previous notations, the mainlobes of both primary frequencies and difference frequencies are marked as ‘M’ in Fig. 12. Grating lobes of the primary frequencies, as well as the eliminated grating lobes of the difference frequencies, are labeled as ‘G1’ and ‘G2’ in Fig. 12. When the mainlobes are steered to -5˚, grating lobe elimination can be observed in Figs. 12(a)-(d). Grating lobes are located at -32˚ and 19˚ in the beampattern of 39.5 kHz in Fig. 12(a), respectively. Grating lobes are located at -31˚ and 18˚ in the beampatterns of 41.5 kHz primary waves, as shown in Fig. 12(b). These grating lobes are not sufficiently separated in angular distance, but still result in grating lobe elimination due to the troughs in the channel directivity of block configuration as shown in Figs. 12(c)-(d). Both results from simulation I and simulation II match the measured beampattern of the difference frequency at the vicinity of mainlobe, as well as the grating lobes. When the steering angle of the primary waves are increased to -10˚ (shown in Figs. 12(e)-(h)), the location of grating lobes are changed to 14˚ and 13˚ in the beampatterns of 39.5 kHz and 41.5 kHz primary waves, respectively (labeled as “G2” in Figs. 12(e)-(f)). Meanwhile, the grating lobes are located at -36˚ in the beampattern of both 39.5 kHz and 40.5 kHz primary wave. The angular distance between the two grating lobes of the primary frequencies remain close to each other. These two grating lobes result in partial grating lobe elimination still due to the channel directivity of block configuration. Figs. 12(g)-(h) show this case of partial grating lobe elimination. Simulation II gives better prediction to the measured amplitude of the eliminated grating lobe than simulation I. Increasing the steering angle of the primary waves to -15˚ leads to a significant decrement of the angular distance between the grating lobes, shown in Figs. 12(i)-(l). In this case, the grating lobes are located close to each other at 9˚ in the beampatterns of 39.5 kHz and 41.5 kHz primary waves (labeled as ‘G1’ in Figs. 12(i)-(j)), which result in spatial aliasing. This grating lobe of the difference frequency wave is shown to be even higher than the mainlobe, as shown in Figs. 12(k)-(l). In this case, partial grating lobe elimination is also observed for the difference frequency wave at 35˚, which is a true elimination that is caused by the angular distance between two grating lobes.

It is shown in Fig. 11 and Fig. 12 that the simulation results match well with the experiment results for the primary frequency waves. However, for the difference frequency wave, product directivity theory

in (6) can only predict the major lobes including the mainlobe, grating lobes and some relatively higher sidelobes. Although many of the sidelobes of the difference frequency wave are clearly observed in the simulation, they are not distinguishable in the experimental plots. A possible reason is the relatively low amplitude of the sidelobes compared to the inherent noise level of the measurement system.

Table I summarizes the locations and amplitudes of grating lobes of parametric loudspeaker for both column-wise and block configurations. The grating lobe elimination for the difference frequency wave is shown to be effective for both configurations in the experiment. For the grating lobe elimination case, experimental results show that the column-wise configuration can reduce the grating lobe (labeled as 'G') by 10.05 dB at the difference frequency of 8 kHz, and the block configuration reduces the grating lobes by 11.99 dB ('G1') and 11.08 dB ('G2') by at the difference frequency of 2 kHz. For the case of partial grating lobe elimination, the column-wise configuration reduces the grating lobe by 8.32 dB at the difference frequency of 4 kHz, and the block configuration reduces the grating lobe by 2.69 dB ('G1') and 3.45 dB ('G2') at the difference frequency of 2 kHz. For the spatial aliasing case, there are no grating lobe eliminations in both column-wise and block configurations. Theoretical simulations can also be used to predict the grating lobe elimination fairly accurately for the above cases.

The grating lobe elimination in the block configuration is observed to be more sensitive to the steering angle and forms two grating lobes in the visible range. However, column-wise configuration can steer to -20˚ with only one grating lobe in the visible range. We can conclude that the column-wise configuration has a better beamsteering capability and grating lobe elimination. But when the steering angle is small, the block configuration can be designed such that the grating lobes coincide with the troughs in its directivity pattern. Thus, the parametric loudspeaker using block configuration is able to achieve very narrow mainlobe, but with limited range of steering angles.

Table I: DISTRIBUTION OF GRATING LOBES IN PARAMETRIC LOUDSPEAKER USING DIFFERENT CONFIGURATIONS (M: Measurement; S: Simulation; S1: Simulation I; S2: Simulation II)

Colum-wise Configuration (refer to Fig. 11)			Block Configuration (refer to Fig. 12)				
	Location of Grating lobe	Reduction of Grating lobe		Location of Grating lobe	Reduction of Grating lobe	Location of Grating lobe	Reduction of Grating lobe

	‘G’ (degree)	‘G’ (dB)		‘G1’ (degree)	‘G1’(dB)	‘G2’(degree)	‘G2’(dB)
Grating lobe elimination case							
8 kHz-M	25	10.05	2 kHz-M	-30	11.99	19	9.41
8 kHz-S1	24	10.37	2 kHz-S1	-31	9.73	18	8.58
8 kHz-S2	25	8.13	2 kHz-S2	-31	10.23	18	9.98
Partial grating lobe elimination case							
4 kHz-M	29	8.32	2 kHz-M	-36	2.69	14	3.45
4 kHz-S1	28	6.12	2 kHz-S1	-36	2.69	13	1.32
4 kHz-S2	29	7.92	2 kHz-S2	-36	16.55	13	10.27
Spatial aliasing case							
1 kHz-M	31	0.35	2 kHz-M	9	0	35	4.98
1 kHz-S1	30	2.07	2 kHz-S1	9	0	34	10.93
1 kHz-S2	30	1.62	2 kHz-S2	9	0	35	5.31

V. CONCLUSION

In this paper, we studied the beamsteering capability for the parametric loudspeaker and its unique property of spatial aliasing. A theoretical model of the beampattern of the parametric loudspeaker was derived based on an equivalent circular Gaussian source array that approximates the directivity characteristics of the linear ultrasonic transducer array. Using the product directivity principle, a digital beamsteerer of the parametric loudspeaker was proposed and implemented in a delay-and-sum structure. The experimental results verified the feasibility of the digital beamsteerer in the parametric loudspeaker. In particularly, this paper also examined the spatial aliasing property of the parametric loudspeaker, and found that different degree of grating lobe elimination can occur under different conditions. It is observed in both simulation and experiment that the occurrence of grating lobe elimination depends on both the difference frequency and the configuration of the ultrasonic transducer array. An important finding of this work is to show that inter-channel spacing of the ultrasonic transducer array in the parametric loudspeaker can be extended to more than $K + 1$ times of half wavelength of lower primary frequency, where K (usually $K = 2$) is the largest index of grating lobes of the lower primary frequency wave in the visible region. When the steering angle is limited to a certain range, the non-aliasing spacing of the ultrasonic transducer array can be further extended. Taking advantage of the increased spacing of the ultrasonic

transducer array, grating lobe elimination allows the parametric loudspeaker to achieve a much shaper mainlobe without increasing the number of channels. This observation will significantly reduce the cost of implementing a steerable parametric loudspeaker. Two configurations of the ultrasonic transducer array were also implemented and compared. The experiments results showed that the column-wise configuration achieves a better beamsteering capability compared to the block configuration. However, in small steering angle applications, block configuration can achieve sharper mainlobe compared to the column-wise configuration when the same numbers of ultrasonic transducers are used in the parametric loudspeaker.

ACKNOWLEDGE

This work is supported by the Singapore National Research Foundation Interactive Digital Media R&D Program, under research grant NRF2007IDM-IDM002-086.

APPENDIX

One important property of the intersection function is that the range of F that ensures the grating lobe elimination of the difference frequency wave does not change with the value of Λ. This property can be proven as follows:

Substitute (7) into (9),

$$I_K(F) = \max_{\Theta} \left\langle \left| \sum_{m=0}^{M-1} w_m \exp\left(j\pi m \frac{\Theta}{\Lambda} \right) \right| \cdot \left| \sum_{m=0}^{M-1} w_m \exp\left\{ j\pi m \frac{F}{\Lambda} \left[\Theta - \min_{\substack{1 \le n_a \le K \\ 1 \le n_b \le L}} \left(\left| n_a \Lambda - \frac{n_b \Lambda}{F} \right| \right) \right] \right\} \right| \right\rangle. \quad \text{(A.1)}$$

Assume Λ is replaced by $\underline{\Lambda}$. Since, both Λ and $\underline{\Lambda}$ are determined, μ is a constant given by $\mu = \underline{\Lambda} / \Lambda$.

Thus, (A.1) can be manipulated as

$$I_K(F) = \max_{\Theta} \left\langle \left| \sum_{m=0}^{M-1} w_m \exp\left(j\pi m \frac{\Theta}{\mu\underline{\Lambda}} \right) \right| \cdot \left| \sum_{m=0}^{M-1} w_m \exp\left\{ j\pi m \frac{F}{\mu\underline{\Lambda}} \left[\Theta - \min_{\substack{1 \le n_a \le K \\ 1 \le n_b \le L}} \left(\left| n_a \mu\underline{\Lambda} - \frac{n_b \mu\underline{\Lambda}}{F} \right| \right) \right] \right\} \right| \right\rangle. \quad \text{(A.2)}$$

For any value of F, there is always a certain Θ that gives the maximum value of the part within the angle brackets. Furthermore, this maximum value is the value of intersection function at this value of F.

Here μ and Θ are known. It is not hard to find $\underline{\Theta} = \mu / \Theta$. Equation (A.2) is further expressed as

$$I_K(F)=\max_{\underline{\Theta}}\left[\left|\sum_{m=0}^{M-1}w_m\exp\left(j\pi m\frac{\underline{\Theta}}{\underline{\Lambda}}\right)\right|\cdot\left|\sum_{m=0}^{M-1}w_m\exp\left[j\pi m\frac{F}{\underline{\Lambda}}\left(\underline{\Theta}-\min_{\substack{1\le n_a\le K\\1\le n_b\le L}}\left(\left|n_a\underline{\Lambda}-\frac{n_b\underline{\Lambda}}{F}\right|\right),\right)\right]\right|\right]. \qquad \text{(A.3)}$$

Equation (A.1) and (A.3) are identical, except that Λ in (A.1) is replaced by $\underline{\Lambda}$ in (A.3), and Θ in (A.1) is replaced by $\underline{\Theta}$ in (A.3). It proves that the maximum values of the part within the angle brackets in (A.1) and (A.3) are the same. Thus, it can be seen that the change of Λ cannot change the range of F that ensures the grating lobe elimination of the difference frequency wave, which is close related to the value of the intersection function.

REFERENCES

[1] C. Shi and W. S. Gan, "Development of Parametric Loudspeaker: A Novel Directional Sound Generation Technology," *IEEE Potentials*, in press.

[2] P. J. Westervelt, "Parametric acoustic array," *J. Acoust. Soc. Amer.*, vol. 35, no. 4, pp. 535-537, 1963.

[3] M. B. Bennett and D. T. Blackstock, "Parametric array in air," *J. Acoust. Soc. Am.*, vol. 57, no. 3, pp. 562-568, 1975.

[4] M. Yoneyama and J. Fujimoto, "The audio spotlight: An application of nonlinear interaction of sound waves to a new type of loudspeaker design," *J. Acoust. Soc. Am.*, vol. 73, no. 5, pp. 1532-1536, 1983.

[5] T. Kamakura, M. Yoneyama, and K. Ikegaya, "Developments of parametric loudspeaker for practical use," in *Proc. Int. Symp. Nonlinear Acoust.*, 1984, pp. 147-150.

[6] T. D. Kite, J. T. Post, and M. F. Hamilton, "Parametric array in air: distortion reduction by preprocessing," in *Proc. 16th Int. Congr. Acoust.*, 1998.

[7] F. J. Pompei, "The use of airborne ultrasonics for generating audible sound beams," *J. Audio Eng. Soc.*, vol. 47, no. 9, pp. 726-731, 1999.

[8] E. L. Tan, P. F. Ji, and W. S. Gan, "On preprocessing techniques for bandlimited parametric loudspeakers," *Applied Acoust.*, vol. 7, no. 5, pp. 486-492, 2010.

[9] M. F. Hamilton and D. T. Blackstock, *Nonlinear Acoustics*, San Diego, CA: Academic Press, 1998.

[10] H. O. Berktay, "Possible exploitation of non-linear acoustics in underwater transmitting applications,"

J. Sound Vib., vol. 2, no. 4, pp. 435-461, 1965.

[11] E. A. Zabolotskaya and R. V. Khokhlov, "Quasi-plane waves in the nonlinear acoustics of confined beams," *Sov. Phys. Acoust.*, vol. 15, pp. 35-40, 1969.

[12] V. P. Kuznetsov, "Equations of nonlinear acoustics," *Sov. Phys. Acoust.*, vol. 16, pp. 467-470, 1971.

[13] M. Zheng and R. F. W. Coates, "The angular response of a parametric array: Analytical solution," *J. Sound Vib.*, vol. 209, no. 3, pp. 493-503, 1998.

[14] M. Zheng and L. S. Wang, "The angular response of a parametric array: General numerical solution," *J. Sound Vib.*, vol. 228, no. 1, pp. 177-197, 1999.

[15] N. Tanaka and M. Tanaka, "Active noise control using a steerable parametric array loudspeaker," *J. Acoust. Soc. Am.*, vol. 127, no. 6, pp. 3526-3537, 2010.

[16] D. Olszewski, F. Prasetyo, and K. Linhard, "Steerable highly directional audio beam loudspeaker", in *Proc. Interspeech*, 2005.

[17] K. S. Tan, W.S. Gan, J. Yang, and M. H. Er, "'An efficient digital beamsteering system for difference frequency in parametric array", in *Proc. IEEE Int. Conf. Acoust. Speech Signal Process.*, 2004.

[18] C. M. Darvennes and M. F. Hamilton, "Scattering of sound by sound from two Gaussian beams," *J. Acoust. Soc. Am.*, vol. 87, no. 5, pp. 1955-1964, 1990.

[19] W. S. Gan, J. Yang, K. S. Tan, M. H. Er, "A digital beamsteerer for difference frequency in parametric array," *IEEE Trans. Audio Speech Lang. Process.*, vol. 14, no. 3, pp. 1018-1025, 2006.

[20] Y. S. Lee, "Numerical solution of the KZK equation for pulsed finite amplitude sound beams in thermoviscous fluids," Ph. D. dissertation, Univ. Texas, Austin, U. S., 1993.

[21] J. J. Wen and M. A. Breazeale, "A diffraction beam field expressed as the superposition of Gaussian beams," *J. Acoust. Soc. Am.*, vol. 83, no. 5, pp. 1752–1756, 1988.

[22] Murata Manufacturing Co. Ltd., Ultrasonic Sensor Application Manual, Oct. 31, 2008. [Online]. Available: http://www.murata.com/products/catalog/pdf/s15e.pdf. [Accessed Jun. 23, 2010].

[23] R. C. Hansen, *Phased Array Antennas*, New Jersey: John Wiley & Sons, 2009.

[24] D. H. Johnson and D. E. Dudgeon, *Array Signal Processing: Concepts and Techniques*, New Jersey:

Prentice Hall, 1993.

Chuang Shi *received his B. Eng. degree in Computer Science and Technology from Beijing Jiaotong University, China in 2005, and his M. Eng. degree in Instrument Science and Technology from Tsinghua University, China in 2008. He is currently pursuing the PhD degree in Electrical and Electronic Engineering in Nanyang Technological University, Singapore.*

Woon-Seng Gan *received his BEng (1st Class Hons) and PhD degrees, both in Electrical and Electronic Engineering from the University of Strathclyde, UK in 1989 and 1993 respectively. He joined the School of Electrical and Electronic Engineering, Nanyang Technological University, Singapore, as a Lecturer and Senior Lecturer in 1993 and 1998 respectively. He is currently an Associate Professor and Deputy Director of the Center for Signal Processing at Nanyang Technological University. His research interests include* adaptive signal processing, active noise control, directional sound system, *and* real-time embedded systems.

Dr. Gan has won the Institute of Engineer Singapore (IES) Prestigious Engineering Achievement Award in 2001 for the work on Audio Beam System. He has published more than 180 international refereed journals and conferences, and has been granted four Singapore and US patents. He has co-authored a book on Digital Signal Processors: Architectures, Implementations, and Applications *(Prentice Hall, 2005). He is also the leading author of a new book on* Embedded Signal Processing with the Micro Signal Architecture, *(Wiley-IEEE, 2007). A new book on* Subband Adaptive Filtering: Theory and Implementation *was also published by John Wiley in August 2009. He is currently a Senior Member of IEEE, Member of Audio Engineering Society and Professional Engineers of Singapore. He is also a member of the Signal Processing Education (SPEd) technical committee of the IEEE Signal Processing Society (USA).*